

SKETCHFFUSION: SKETCH-GUIDED IMAGE EDITING WITH DIFFUSION MODEL

Weihang Mao* Bo Han* Zihao Wang

Zhejiang University, Hangzhou, China

ABSTRACT

Sketch-guided image editing aims to achieve local fine-tuning of the image based on the sketch information provided by the user while maintaining the original status of the unedited areas. Due to the high cost of acquiring human sketches, previous works mostly relied on edge maps as a substitute for sketches, but sketches possess more rich structural information. In this paper, we propose a sketch generation scheme that can preserve the main contours of an image and closely adhere to the actual sketch style drawn by the user. Simultaneously, current image editing methods often face challenges such as image distortion, training cost, and loss of fine details in the sketch. To address these limitations, We propose a conditional diffusion model (SketchFFusion) based on the sketch structure vector. We evaluate the generative performance of our model and demonstrate that it outperforms existing methods.

Index Terms— Image editing, diffusion model

1. INTRODUCTION

AIGC technology is gradually impacting the ways digital content is produced and consumed. Recently, methods based on diffusion models have made significant breakthroughs in the task of text-to-image generation, with many powerful models [1, 2] enabling the public to easily realize AI painting. However, the details of images generated from complex texts are often less than ideal, requiring users to make secondary modifications. Compared to other editing conditions such as text and audio, sketches accurately reflect the image regions and corresponding shape structures that people want to modify.

Presently, the majority of sketch-guided image editing methods [3, 4, 5, 6, 7] have shifted to image restoration tasks based on sketch conditions. Although much work [8, 9, 10] has been done in the image restoration task, there are still many challenges in the task of sketch-guided image editing:

- Infinite possible mappings between multidimensional degraded observations and restored images determine the ill-posed nature of such inverse problems [11].
- The repaired image region must maintain consistency in semantics and style with the rest of the image [12].

- The edges of the image area to be repaired must undergo smoothing treatment to avoid distortion [13]. But the specific details of a sketch can easily be lost.

Building on the foundation of image restoration, sketch-guided image editing involves sketches into the region of the mask image, such that the repaired region in the image encompasses the shape and structure information added by the sketch, thereby realizing the desired editing effect on the image. FaceShop [5] innovatively decomposes the sketch-guided image editing task into two sub-tasks: image restoration and image translation, and jointly trains the two network models. However, it must resize the restored local patch to accept fitting input dimensions, and the resizing process would distort the information in both the erased and remaining portions of the image. SC-FEGAN [3] adheres to the framework of FaceShop, but optimizes the issue of large, easily distorted, and inconsistent editing regions present in FaceShop by incorporating an additional style loss. DeepPS [6] optimizes robustness with respect to the sketch input. But they often merge lines that are close to each other, which inevitably loses some structural details. Deepfill-V2 [7] introduces a gated neural network to process the input images, sketches, and masks, and trains the model through adversarial learning. However, since it does not use color input, the color in the synthesized image is generated by inference from the prior distribution learned from the training data set. At the same time, due to the difficulty of collecting pairs of sketches and color images as training data, existing works [3, 5, 14] typically exploit edge maps as real sketches. Despite certain success in shoe, handbag, and face synthesis, edge maps look apparently different from human sketches, the latter often being more causal, varied, or even wild.

To deal with the lack of human sketches limitations, we propose a framework for paired data generation of human sketches and color images. We first extract the edge grayscale image from the RGB image. Taking into account both the style of the human sketch and the model’s training, we choose an appropriate threshold to generate the binarized sketch. Additionally, we propose a random mask image generation method so that the generated mask images are as close as possible to human habits. To reduce model training time and reinforce sketch condition information, we propose an image editing framework. We first utilize the autoencoder to transform images from high-dimensional space to low-

* Equal contribution <https://borishanzju.github.io/SketchFFusion/>

dimensional latent space, and then construct a conditional diffusion model based on the latent space. With the aid of the autoencoder, we alleviate the problem of detail loss during conditional input.

In summary, we make the following contributions:

- We propose a sketch generation framework that retains the primary contour of the original image and adheres to the user’s actual drawing style.
- We propose a sketch-guided image editing method, which greatly reduces the cost of model training while reinforcing the line contour information.

2. BACKGROUND

Image Restoration. Since the advent of GANs, many image restoration models based on GANs have improved compared to traditional graphic-based methods [15, 16]. ContextEncoder [17] first proposes a GAN-based image restoration framework, designing a loss for the realism of the repaired image. Many studies have optimized based on it, MEDFE [10] adopts an encoder-decoder structure to fuse structure and texture information of images at different scales. DMFN [18] incorporates dilated convolution layers in its encoder to acquire a larger view, and employs a regression loss to enhance semantic constraints on the missing regions. A pyramidal structure is proposed by PEN-Net [19], establishing the connection between the feature maps containing high-level semantics and low-level image information through an attention mechanism, thus achieving a balance between visual effect and semantic coherence. SN-PatchGAN [7] introduces a gated neural network and inputs an additional mask as a separate channel into the network, allowing the model to support repair regions with more flexible shapes. The diffusion model, as an alternative to GAN, has superior performance. RePaint [20] employs an iterative resampling method, which integrates more global semantic information in the repair region.

Sketch-based Image Editing. Many sketch-guided image editing models are founded upon the image restoration framework. FaceShop [5] employs a combined framework of image restoration and image translation to realize sketch-guided editing. Beyond the input of the image to be edited, the sketch, and the mask image, the input also includes a color image to support color guidance information. Additionally, FaceShop inputs an extra random noise image to enhance the generation of finer textures by the network model. SC-FEGAN [3] assesses the style between the generated image and the real image using the Gram matrix, thereby alleviating the issue of inconsistent distortion caused by extensive editing. DeepPS [6] employs dilation operations on sketches, enhancing the model’s generalization capabilities towards hand-drawn sketch inputs. DeFLONet [4] alleviates the semantic decay of guidance information by incorporating a generative

block in each convolutional layer, which directly injects guidance information. SketchEdit [21] proposes mask-free local image manipulation, which only requires sketch inputs from users and utilizes the entire original image.

3. SKETCH GENERATION FRAMEWORK

For sketch generation, it is crucial to maintain the primary contours of the original image while adhering to the user’s actual sketching style. We adopt the LDC model [22] to extract the image edges, resulting in a corresponding grayscale image. Subsequently, an appropriate threshold (TH) is selected for binarization and inversion, thereby ensuring that the sketch aligns with the practical human sketch. A higher threshold value will preserve more details in the contours, while a lower threshold value will omit finer sketch outlines, as shown in Fig. 1 (a). In our case, we choose a high threshold value of 125, which aligns with the user’s drawing habits.

For mask generation, the following elements should be taken into account: 1) the mask shape should ensure diversity to prevent overfitting in the model’s training. 2) the mask shape should align with the user’s actual drawing style. 3) the mask generation should be simple, to avoid negatively impacting the training efficiency. The generation of the mask image is divided into two parts: firstly, simulate the rectangle selection by generating rectangles randomly, and secondly, simulate the eraser-like selection by moving circular regions. After generating the respective mask images using these two algorithms, we combine them to obtain the final mask image.

For an image sample X , we first randomly generate a mask image M . The image obtained by multiplying X with $1 - M$, denoted as X_M , serves as the image to be edited. The image obtained by multiplying sketch image maS with M , denoted as S_M , serves as the sketch image for the region to be repaired. M is used as the region identifier for the image to be edited, and X_M , S_M , and M are all input to the model, with the original image X serving as the ground truth (GT) for the image editing guided by the sketch, as shown in Fig. 1 (b).

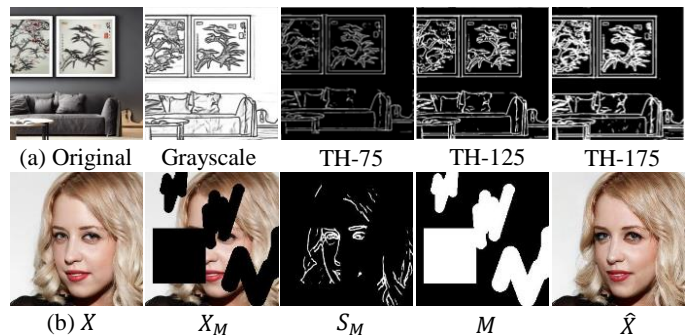


Fig. 1. (a) Sketch generation with different thresholds. (b) X_M , S_M , M : condition image. \hat{X} : generated image. X : GT.

4. SKETCHFUSION METHOD

The schematic overview of our proposed architecture is illustrated in Fig. 2. It mainly consists of four components: image autoencoder, sketch autoencoder, diffusion process, and denoising process.

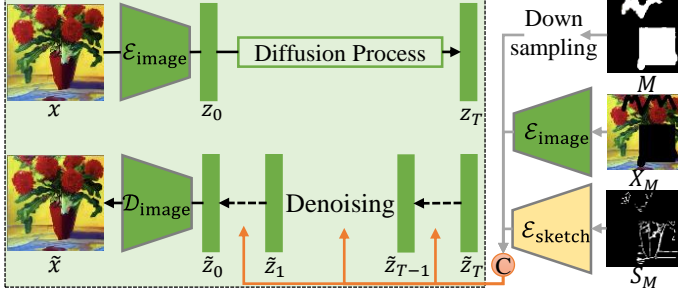


Fig. 2. An overview of our proposed model

We refer to the VQGAN model [23] to build the image autoencoder and sketch autoencoder to effectively reduce the dimensionality of features for image samples and sketch samples. The VQGAN model is mainly composed of three parts: encoder \mathcal{E} , decoder \mathcal{D} , and discriminator \mathcal{N} . After inputting the image sample $x \in \mathbb{R}^{H \times W \times d}$ to the encoder, the hidden layer vector $z \in \mathbb{R}^{h \times w \times d}$ is obtained, where $W/w = H/h = f$ indicates the downsampling scale factor. Subsequently, load the hidden layer vector z into the codebook for vector quantization. The codebook stores a series of discretized vectors, which can be expressed as $\mathcal{Z} = \{z_k\}_{k=1}^K \in \mathbb{R}^{h \times w \times d}$, where K is the number of discretized vectors. The role of the codebook is equivalent to cluster hidden vectors, which can make the reconstruction more stable. The vector quantization is to obtain the vector \hat{z} closest to z by querying the codebook. The structure of the decoder is similar to the encoder, which upsamples the vector \hat{z} to the reconstructed sample \tilde{x} . The training objective of the model is to minimize the reconstruction error and maximize the adversarial loss:

$$L = \min_{\mathcal{E}, \mathcal{D}} \max_{\mathcal{N}} L_{rec}(x, \mathcal{D}(\mathcal{E}(x))) + L_{GAN} \quad (1)$$

$$L_{rec} = \sum_{n=1}^N \|x - \mathcal{D}(\mathcal{E}(x))\|^2 \quad (2)$$

$$L_{GAN} = \log(\mathcal{N}(x)) + \log(1 - \mathcal{N}(\tilde{x})) \quad (3)$$

For the RGB image sample x and the sketch sample s_{mask} , we pre-train two autoencoders, $model_{image}$ and $model_{sketch}$, respectively. The $model_{image}$ is composed of an image encoder \mathcal{E}_{image} and an image decoder \mathcal{D}_{image} . The $model_{sketch}$ is composed of a sketch encoder \mathcal{E}_{sketch} and a sketch decoder \mathcal{D}_{sketch} . The structure of $model_{image}$ and $model_{sketch}$ is based on the above VQGAN model, and the specific parameters are shown in Table 1.

| Model | Input | Hidden Vector | Scale Factor |
|------------------|---------------------------|-------------------------|--------------|
| $model_{image}$ | $256 \times 256 \times 3$ | $64 \times 64 \times 3$ | 4 |
| $model_{sketch}$ | $256 \times 256 \times 1$ | $64 \times 64 \times 1$ | 4 |

Table 1. Pretrained autoencoder parameters

We apply the image encoder \mathcal{E}_{image} to obtain the x_{mask} conditional feature $c_{image} \in \mathbb{R}^{64 \times 64 \times 3}$ and use the sketch encoder \mathcal{E}_{sketch} to get the s_{mask} conditional feature $c_{sketch} \in \mathbb{R}^{64 \times 64 \times 3}$. For the $mask$ condition, since it contains less detailed information than x_{mask} and s_{mask} , we directly down-sample it to obtain the conditional feature $c_{mask} \in \mathbb{R}^{64 \times 1 \times 1}$. Finally, we concatenate them as the whole condition.

Diffusion Process: We first encode x into the hidden vector $z = \mathcal{E}_{image}(x)$, and then add noise to z . The representation of z on time step t is denoted as z_t . Where $\bar{\alpha}_t = \prod_{i=1}^t \alpha_i$, $\alpha_t = 1 - \beta_t$ and β_t are pre-defined.

$$z_t = \sqrt{\bar{\alpha}_t} \mathcal{E}_{image}(x) + \sqrt{1 - \bar{\alpha}_t} \epsilon_t \quad (4)$$

Denoising Process: It can be represented as:

$$\begin{aligned} p_{\theta}(z_{t-1} | z_t, c_{image}, c_{sketch}, c_{mask}) = \\ \mathcal{N}(z_{t-1}; \mu_{\theta}(z_t, t, c_{image}, c_{sketch}, c_{mask}), \\ \Sigma_{\theta}(z_t, t, c_{image}, c_{sketch}, c_{mask})) \end{aligned} \quad (5)$$

During model training, the model predicts the accumulated noise $\epsilon_{\theta} = \epsilon_{\theta}(x_t, t, c_{image}, c_{sketch}, c_{mask})$ at each time step t of the denoising process and the mean squared error between ϵ_{θ} and the actually added noise $\epsilon_t \sim \mathcal{N}(0, \mathbf{I})$ is calculated as the model's loss function:

$$L_{latent} = \frac{\|\epsilon - \epsilon_{\theta}\|^2}{N} \quad (6)$$

Where, $\epsilon_{\theta} = \epsilon_{\theta}(z_t, t, c_{image}, c_{sketch}, c_{mask})$, N is the number of elements in ϵ_{θ} .

During inference with the $model_{latent}$, first, $\tilde{z}_T \sim \mathcal{N}(0, \mathbf{I})$ is obtained by sampling from random noise. For $t = T, \dots, 1$, $\tilde{z}_{t-1} \sim p_{\theta}(\tilde{z}_{t-1} | \tilde{z}_t, c_{image}, c_{sketch}, c_{mask})$ is iteratively sampled to obtain \tilde{z}_0 :

$$\begin{aligned} \tilde{z}_{t-1} = \frac{1}{\sqrt{\alpha_t}} \left(\tilde{z}_t - \frac{\beta_t}{\sqrt{1 - \bar{\alpha}_t}} \epsilon_{\theta}(\tilde{z}_t, t, c_{image}, c_{sketch}, c_{mask}) \right) \\ + \sigma_t \mathbf{z} \end{aligned} \quad (7)$$

Where $\mathbf{z} \sim \mathcal{N}(0, \mathbf{I})$. Finally, utilizing the decoder \mathcal{D}_{image} corresponding to \mathcal{E}_{image} , the image \tilde{x} is decoded from \tilde{z}_0 .

5. EXPERIMENTS

5.1. Dataset

To compare with existing SOTA methods [3, 6, 7], we conducted training and evaluation on the CelebA-HQ dataset.

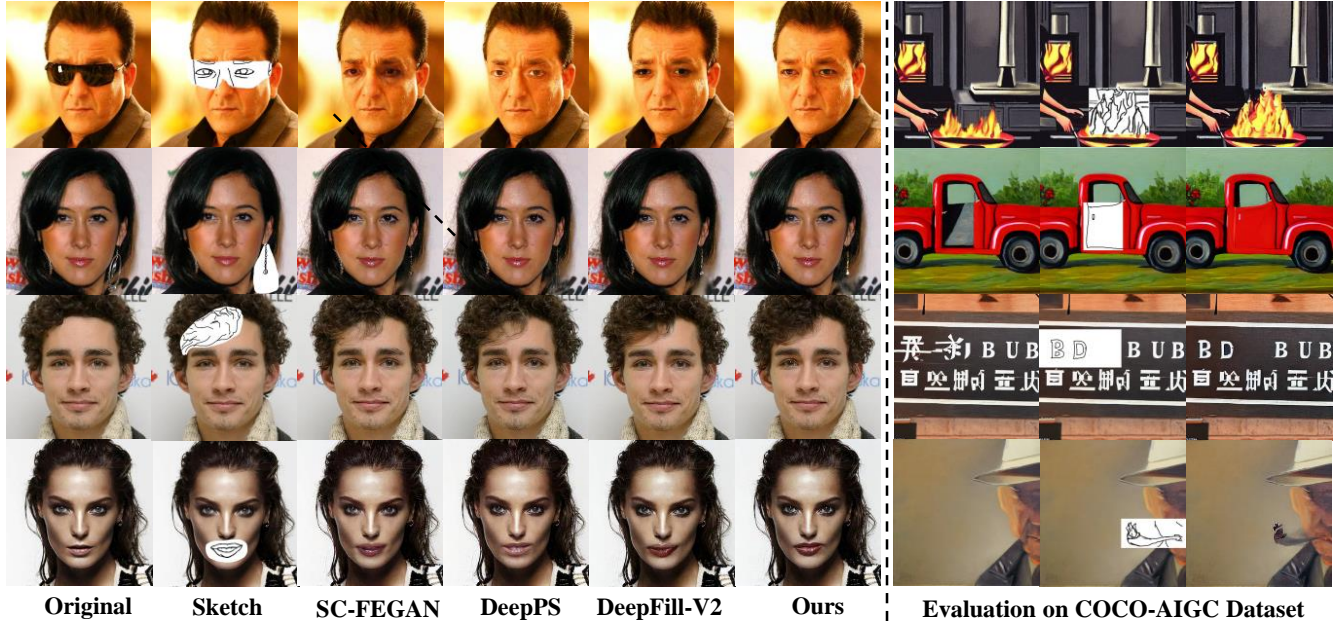


Fig. 3. Visualization results on CelebA-HQ dataset and COCO-AIGC dataset

| Category | COCO Dataset | AIGC Dataset | Total |
|----------|--------------|--------------|--------|
| Train | 153284 | 583617 | 736904 |
| Test | 10673 | 20015 | 30688 |

Table 2. The details of COCO dataset and AIGC dataset

The CelebA-HQ dataset is a facial dataset comprised of 30,003 images of resolution 1080×1080 . The training set contains 28,003 images, while the validation set consists of 2,000 images. To ensure fairness in the evaluation, we adopt the same data set partitioning method.

The above methods [3, 6, 7] are only trained and evaluated on the CelebA-HQ dataset, with only pre-trained model publicly available. To verify the effectiveness of our proposed method on images of different categories, we constructed a multi-style AIGC dataset using the LDM model [2] based on the COCO dataset, and separately trained and evaluated our proposed method on the COCO-AIGC dataset. The COCO dataset contains 123,287 images covering most scenes and objects in everyday life. In addition, the dataset includes text descriptions corresponding to the image data. Based on the text descriptions in the COCO dataset, we added additional style descriptions to generate a multi-style AIGC dataset. The details of the COCO-AIGC dataset are shown in Table 2.

5.2. Results

We adopt FID, PSNR, and SSIM as objective evaluation metrics, and the evaluation results on the CelebA-HQ dataset are shown in Table 3. It can be seen that our method outper-

| Method | FID↓ | PSNR↑ | SSIM↑ |
|-----------------|-------------|--------------|---------------|
| SC-FEGAN [3] | 11.72 | 24.27 | 0.8740 |
| DeepPS [6] | 11.42 | 24.56 | 0.8677 |
| DeepFill-V2 [7] | 14.38 | 24.11 | 0.8008 |
| Ours | 9.07 | 26.74 | 0.8822 |

Table 3. Objective evaluation results on CelebA-HQ dataset

forms the other methods. Meanwhile, as can be seen from Fig. 3, the generated images in this paper have better consistency in style and representation of details. Furthermore, we conducted training and evaluation on the COCO-AIGC dataset individually, as shown in Fig. 3. The results indicate that our proposed method is still capable of generating images that adhere to the structural details of the sketches.

6. CONCLUSION

In this paper, we propose a sketch generation framework to address the issue of scarce human sketches, which can effectively simulate the human sketch drawing style while fully preserving the structural details. To tackle the problem of distorted image edges, we introduce a sketch-guided image editing model (SketchFFusion) that strengthens the sketch condition while significantly reducing the training time and memory consumption of the diffusion model itself. However, the model proposed currently only supports binary sketches as input and cannot handle colored sketches. In the future, we will incorporate colored sketches to achieve color editing.

7. REFERENCES

- [1] Alex Nichol, Prafulla Dhariwal, Aditya Ramesh, Pranav Shyam, Pamela Mishkin, Bob McGrew, Ilya Sutskever, and Mark Chen, “Glide: Towards photorealistic image generation and editing with text-guided diffusion models,” *arXiv preprint arXiv:2112.10741*, 2021.
- [2] Robin Rombach, Andreas Blattmann, Dominik Lorenz, Patrick Esser, and Björn Ommer, “High-resolution image synthesis with latent diffusion models,” in *CVPR*, 2022, pp. 10684–10695.
- [3] Youngjoo Jo and Jongyoul Park, “Sc-fegan: Face editing generative adversarial network with user’s sketch and color,” in *ICCV*, 2019, pp. 1745–1753.
- [4] Hongyu Liu, Ziyu Wan, Wei Huang, Yibing Song, Xintong Han, Jing Liao, Bin Jiang, and Wei Liu, “Deflo-net: Deep image editing via flexible low-level controls,” in *CVPR*, 2021, pp. 10765–10774.
- [5] Tiziano Portenier, Qiyang Hu, Attila Szabo, Siavash Arjomand Bigdeli, Paolo Favaro, and Matthias Zwicker, “Faceshop: Deep sketch-based face image editing,” *arXiv preprint arXiv:1804.08972*, 2018.
- [6] Shuai Yang, Zhangyang Wang, Jiaying Liu, and Zongming Guo, “Deep plastic surgery: Robust and controllable image editing with human-drawn sketches,” in *Computer Vision—ECCV 2020: 16th European Conference, Glasgow, UK, August 23–28, 2020, Proceedings, Part XV 16*. Springer, 2020, pp. 601–617.
- [7] Jiahui Yu, Zhe Lin, Jimei Yang, Xiaohui Shen, Xin Lu, and Thomas S Huang, “Free-form image inpainting with gated convolution,” in *ICCV*, 2019, pp. 4471–4480.
- [8] Zhendong Wang, Xiaodong Cun, Jianmin Bao, Wengang Zhou, Jianzhuang Liu, and Houqiang Li, “Uformer: A general u-shaped transformer for image restoration,” in *CVPR*, 2022, pp. 17683–17693.
- [9] Syed Waqas Zamir, Aditya Arora, Salman Khan, Munawar Hayat, Fahad Shahbaz Khan, Ming-Hsuan Yang, and Ling Shao, “Multi-stage progressive image restoration,” in *CVPR*, 2021, pp. 14821–14831.
- [10] Hongyu Liu, Bin Jiang, Yibing Song, Wei Huang, and Chao Yang, “Rethinking image inpainting via a mutual encoder-decoder with feature equalizations,” in *Computer Vision—ECCV 2020: 16th European Conference, Glasgow, UK, August 23–28, 2020, Proceedings, Part II 16*. Springer, 2020, pp. 725–741.
- [11] Jingwen Su, Boyan Xu, and Hujun Yin, “A survey of deep learning approaches to image restoration,” *Neuro-computing*, vol. 487, pp. 46–65, 2022.
- [12] Omar Elharrouss, Noor Almaadeed, Somaya Al-Maadeed, and Younes Akbari, “Image inpainting: A review,” *Neural Processing Letters*, vol. 51, pp. 2007–2028, 2020.
- [13] Zhen Qin, Qingliang Zeng, Yixin Zong, and Fan Xu, “Image inpainting based on deep learning: A review,” *Displays*, vol. 69, pp. 102028, 2021.
- [14] Phillip Isola, Jun-Yan Zhu, Tinghui Zhou, and Alexei A Efros, “Image-to-image translation with conditional adversarial networks,” in *CVPR*, 2017, pp. 1125–1134.
- [15] Connelly Barnes, Eli Shechtman, Adam Finkelstein, and Dan B Goldman, “Patchmatch: A randomized correspondence algorithm for structural image editing,” *ACM Trans. Graph.*, vol. 28, no. 3, pp. 24, 2009.
- [16] Patrick Perez, Michel Gangnet, and Andrew Blake, “Patchworks: Example-based region tiling for image editing,” *Microsoft Research, Redmond, WA, Tech. Rep. MSR-TR-2004-04*, pp. 1–8, 2004.
- [17] Deepak Pathak, Philipp Krahenbuhl, Jeff Donahue, Trevor Darrell, and Alexei A Efros, “Context encoders: Feature learning by inpainting,” in *CVPR*, 2016, pp. 2536–2544.
- [18] Zheng Hui, Jie Li, Xiumei Wang, and Xinbo Gao, “Image fine-grained inpainting,” *arXiv preprint arXiv:2002.02609*, 2020.
- [19] Yanhong Zeng, Jianlong Fu, Hongyang Chao, and Bain-ing Guo, “Learning pyramid-context encoder network for high-quality image inpainting,” in *CVPR*, 2019, pp. 1486–1494.
- [20] Andreas Lugmayr, Martin Danelljan, Andres Romero, Fisher Yu, Radu Timofte, and Luc Van Gool, “Repaint: Inpainting using denoising diffusion probabilistic models,” in *CVPR*, 2022, pp. 11461–11471.
- [21] Yu Zeng, Zhe Lin, and Vishal M Patel, “Sketchedit: Mask-free local image manipulation with partial sketches,” in *Proceedings of the IEEE/CVF Conference on Computer Vision and Pattern Recognition*, 2022, pp. 5951–5961.
- [22] Xavier Soria, Gonzalo Pomboza-Junez, and Angel Domingo Sappa, “Ldc: Lightweight dense cnn for edge detection,” *IEEE Access*, vol. 10, pp. 68281–68290, 2022.
- [23] Patrick Esser, Robin Rombach, and Bjorn Ommer, “Taming transformers for high-resolution image synthesis,” in *CVPR*, 2021, pp. 12873–12883.